Applied Physics Express

The Japan Society of Applied Physics

LETTER

Angular distribution measurement of high-energy argon neutral and ion in a 13.56 MHz capacitively-coupled plasma

To cite this article: Keita Ichikawa *et al* 2021 *Appl. Phys. Express* **14** 126001

Applied Physics Express 14, 126001 (2021) LETTER
https://doi.org/10.35848/1882-0786/ac33c4

Angular distribution measurement of high-energy argon neutral and ion in a 13.56 MHz capacitively-coupled plasma

Keita Ichikawa[1*], Manh Hung Chu[1], Makoto Moriyama[1], Naoya Nakahara[1], Haruka Suzuki[1,2], Daiki Iino[3], Hiroyuki Fukumizu[3], Kazuaki Kurihara[3], and Hirotaka Toyoda[1,2,4*]

[1]Department of Electronics, Nagoya University, Furo-cho, Chikusa-ku, Nagoya 464-8603, Japan
[2]Center for Low Temperature Plasma Sciences, Nagoya University, Furo-cho, Chikusa-ku, Nagoya 464-8603, Japan
[3]Institute of Memory Technology Research & Development, Kioxia Corp. Isogo-ku Yokohama, 235-0017, Japan
[4]National Institute for Fusion Science, 322-6, Oroshi, Toki, 509-5292 Japan

*E-mail: ichikawa.keita@a.mbox.nagoya-u.ac.jp; toyoda@nuee.nagoya-u.ac.jp

Received September 28, 2021; revised October 18, 2021; accepted October 27, 2021; published online November 10, 2021

Angular distributions of high energy neutrals and ions, impinging on an RF-biased electrode in a 13.56 MHz capacitively-coupled argon plasma were investigated. Ions and neutrals were introduced into a drift chamber that was directly connected to the RF electrode. A two-dimensional beam image was measured by a micro-channel plate. Neutral and ion beams were separated by an electrostatic deflector in the drift chamber. Angular distribution widths for ion and neutral were less than 1° at self-bias voltages above 300 V and monotonically decreased with increasing the self-bias voltage. Neutral angular distribution width was larger than that of ion, irrespective of self-bias voltage.

Anisotropic etching is one of the essential processes in the fabrication of nanoscale or three-dimensional semiconductor devices. This process utilizes bombardment of directional high-energy ions accelerated by the sheath, where ions assist surface chemical reactions with the help of neutral radicals. In the plasma etching process, resist patterns are transferred to the wafer by anisotropy of ions impinging on the wafer surface. However, various undesirable etching features sometimes happen such as notching,[1,2] sidewall bowing,[3–7] micro trenching at the sidewall base.[6–10] These features occur by charging on the bottom of the hole,[11,12] or broadening of ion angular distribution (IAD). In the recent trend of high aspect hole etching with aspect ratios of ∼100, understanding of not only IAD but also neutral angular distribution (NAD) becomes more important.

So far, various works have been reported to investigate ion behavior in the sheath,[13–15] the ion angular distribution function (IADF), and neutral angular distribution function (NADF)[16–22] using different analytical and numerical models. Gottscho calculated the IADF using the sheath voltage and ion velocity distribution at the sheath edge.[15] Mizutani and Hayashi measured ion energy distribution function (IEDF) and calculated neutral energy distribution function (NEDF) as well as IADF and NADF. Raja and Linne considered ion motion within the sheath under the influences of electron temperature, ion density, bias voltage, and bias frequency.[17] Wang et al. developed a hybrid model that consists of a fluid model for plasma simulation and a Monte Carlo for tracking the ions and neutrals passing through the sheath. In a 30 MHz/2 MHz dual-frequency plasma, they have found that almost all ions impinge on the substrate at angles less than 4° off normal direction and that the angular distribution of fast neutrals is strongly correlated with that of ions.[18] The influence of superposing a low-frequency bias voltage onto the rf-powered electrode on the IADF has also been examined by Takao and co-workers.[21]

In parallel with the simulation, attempts to investigate IADF from experiments have been also reported. An angular analyzer consisting of annular collection rings was employed by some groups[23–26] to measure the IADF. Nonetheless, due to the electrical nature of the analyzer, this technique is incapable to measure the angular distribution of neutral species. Furthermore, the physically discrete collection rings are difficult to obtain better than angular resolutions below the order to several degrees.[23] As an alternative method of the IADF measurement, Aydil et al. utilized a microchannel plate (MCP) coupled with a phosphor screen to visualize the angular distribution of particles with resolutions less than 0.5°.[27] However, they measured only IADF on the grounded surface and did not measure the IADF on the RF-biased surface. Furthermore, they did not mention the results of NADF, presumably due to the lack of neutral kinetic energy to be detected by the MCP.

In this study, we report the first measurement of NADF, as well as IADF, impinging on the RF-powered electrode in a 13.56 MHz capacitively coupled argon plasma. Particles are extracted from the plasma through a sampling orifice. A drift tube is directly connected to the RF electrode and, after particles travel through a drift tube, they are detected by an MCP assembly with a phosphorus screen. Light emission from the phosphorus screen is captured by an ICCD camera. Ion and neutral angular distributions are measured varying the RF power.

Figure 1 shows a schematic of the experimental setup. A discharge chamber (diameter: 30 cm, length: 23 cm) is evacuated by a turbomolecular pump at a base pressure of $\sim 10^{-4}$ Pa. Ar gas is fed to the chamber through a mass flow controller at a pressure (p) of 4.0 Pa. Plasma is produced by 13.56 MHz RF power (P_{RF}, <400 W) applied to an RF electrode (diameter: 10 cm). Plasma parameters are measured by an RF-compensated wire-type Langmuir probe (diameter: 0.1 mm, length: 5 mm) which is placed 2.5 cm away from the center of the RF electrode. Plasma density (n_0) is 1.5 to 2.2×10^{15} m^{-3} at RF powers from 100 W to 400 W. The electron temperature (T_e) and plasma potential (V_P) are 17 V and 3.5 eV, respectively, and are almost constant with respect to the RF power. RF peak-to-peak voltage (V_{PP}) and DC self-bias voltage (V_{DC}) of the RF electrode are monitored by a high-voltage probe. Hereafter negative self-bias voltage is indicated by its absolute value.

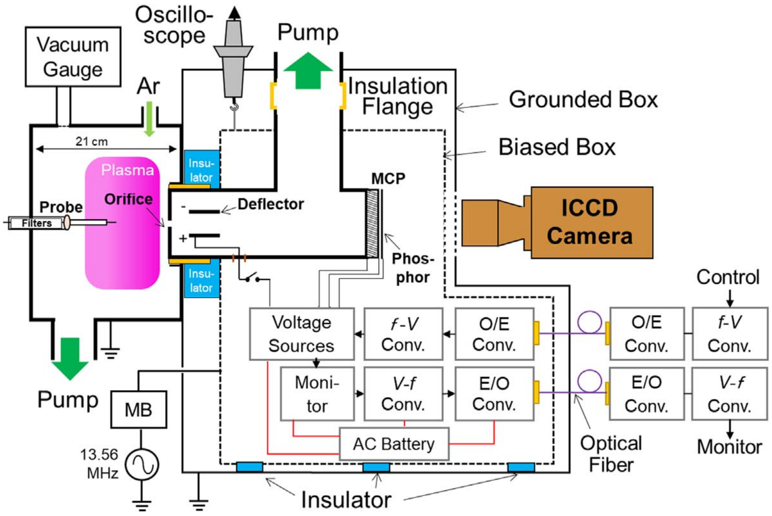

Fig. 1. (Color online) Schematic of the experimental setup.

For angular distribution measurements of ions and neutrals, a drift chamber (diameter: 10 cm, length: 29 cm) is connected to the RF electrode. Ions and neutrals are extracted from the plasma through an orifice (diameter: 27 μm, thickness: 0.25 mm) made of stainless steel at the center of the RF electrode. The drift chamber is directly connected to the RF electrode and is evacuated by another turbomolecular pump. Under the discharge condition, pressure in the drift chamber is below $\sim 5 \times 10^{-5}$ Pa, which is low enough to realize collision-free space. Angular distributions of high-energy ions and neutrals are measured by an MCP with a phosphor plate, which is placed 29 cm away from the orifice. The potential of the MCP front-side is the same as that of the drift chamber. The backside of the MCP and phosphor plate are positively biased with respect to the MCP front-side at +1 kV and + 5 kV, respectively. To separate the ion beam from the neutral beam, a pair of deflector plates (electrode length: 33 mm, electrode spacing: 5 mm) is placed in the vicinity of the orifice. By applying positive ($+V_{DEF}/2$) and negative ($-V_{DEF}/2$) voltages to the electrodes, the space potential at the center of the electrode spacing is the same as that of the drift chamber.

To confirm the accuracy of the angular distribution measurement, the drift chamber is carefully arranged. In the drift chamber, electric-field-free space is realized (except for the deflecting electric field), by letting the drift chamber potential to that of the RF electrode. This configuration, however, means that all the voltage sources connected to the drift chamber should be RF-biased as well as the RF electrode. For this purpose, power supplies of the MCP and the deflector, as well as the drift chamber, are placed in a metal box (RF-biased box) and are covered with a shield box. Voltage sources for the deflector and the MCP are operated by a battery-based AC power supply in the RF box. Voltages are controlled and monitored through optical fibers with signal converters. Beam profiles of ion and neutral on the MCP are converted into light images by the phosphor plate and are monitored by an ICCD camera through a shield-mesh.

Imaging of ion and neutral spots on the MCP enables us to obtain reliable data for the angular distribution. The high spatial resolution of the MCP (25 μm) and long-distance between the orifice and the MCP realize a high angular resolution of $\sim 0.01°$. The influence of UV light on the MCP is negligible because the MCP is sensitive only to deep UV light (<120 nm) and is not sensitive to the UV light emission from the Ar plasma. The Space-charge electric field of the ion beam might influence the angular distribution. However, the estimated potential of the ion beam at the lowest V_{DC} in this study ($V_{DC} = 200$ V) is $\sim$1 mV, which is much lower than typical ion thermal energies[28] and this factor is negligible in this study. The influence of the orifice aspect ratio might be another factor, but transmittance of the orifice in this study is 0.95 at an incident angle of 1° from the surface normal, and this factor is also negligible.

To separate the neutral signal from the measured beam spot, the ion deflector is used. Figure 2 shows an example of a beam image at $P_{RF} = 200$ W, which corresponds to $V_{DC} = 640$ V. V_{DEF} is varied from 0 to 8 V, as shown in Figs. 2(a)–2(c), respectively. In the figure, the x axis is defined as the direction parallel to the electric field of the ion deflector. Dotted circles in the figures indicate the periphery of the MCP. By applying the deflector voltage, one spot is separated into two spots, one is at the center and another is to the right side (direction to the negative voltage deflection electrode). From this, deflected spot and center spots are confirmed to be positive ion beam and neutral beam, respectively. In Fig. 2(c), deflected ion spot is not circular but is slightly broad to the right side with a weaker signal. This structure suggests that the maximum ion intensity exists at the maximum energy of the ion energy distribution (IED) and the ion intensity gradually decreases at low ion energies. Here, a deflected distance of the ion (X_S) is defined as the distance between the center of the neutral spot and the ion beam position of its maximum intensity. X_S was measured as a function of V_{DEF} at $P_{RF} = 200$ W. The X_s monotonically increased and was $\sim$15 mm at $V_{DEF} = 8$ V. To elucidate the ion energy from the ion peak, a three-dimensional ion trajectory simulation was carried out, changing ion energy and V_{DEF}. The best-fitted simulated ion energy was $\sim$660 V, which was almost the same as the ion energy evaluated from the measured V_{DC} and V_P. As is well known, the ion energy distribution at an RF electrode has a "saddle-like" structure due to oscillating sheath.[28,29] From measured RF voltage

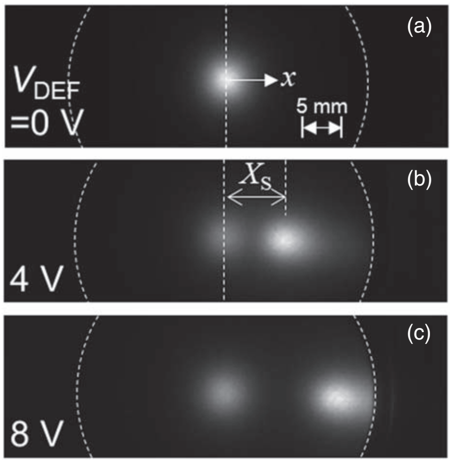

Fig. 2. (Color online) Beam spot images obtained by the MCP. Deflector voltages are (a) 0 V, (b) 4 V, and (c) 8 V. RF power and Ar pressure are 200 W and 4 Pa, respectively.

amplitude and sheath thickness estimated from the plasma density at $P_{RF} = 200$ W, energy deviation ($\Delta\varepsilon_i$) from the center of the "saddle" ($\bar{\varepsilon}$) was estimated to be $\Delta\varepsilon_I/\bar{\varepsilon} \sim 0.1$, which corresponds to the deviation of peak position $\Delta X_s \sim 1.5$ mm at $V_{DEF} = 8$ V in Fig. 2(c). The IED is also influenced by charge exchange (CX) collisions in the sheath, which produces low-energy ions besides the peak corresponding to the V_{DC}. The energy spread toward lower ion energies is considered to be mainly due to energy broadening by the oscillating sheath and CX collisions of the ions in the sheath.

Figures 3(a) and 3(b) show semi-logarithmic plots of angular profiles for ion and neutral, respectively, at RF powers from 50 to 400 W. Incident angles of particles (θ_{in}) are obtained using the distance of the MCP from the orifice (L_D) and position from the spot center x on the MCP. Ion angular profile was obtained by subtracting beam profiles with the deflector is off by those with the deflector is on, i.e., neutral beam profile at the center. In Fig. 3, part of angular profiles on the right side is omitted because the profiles are disturbed by the residual ion signal component. Both in Figs. 3(a) and 3(b), their peak intensities monotonically increase with increasing the RF power. Their angular profiles show steep peak components ($|\theta| \lesssim 0.7°$ for ion profile and $|\theta| \lesssim 1°$ for neutral profile) and low-intensity broad components at larger angles. These angular profiles are presumably

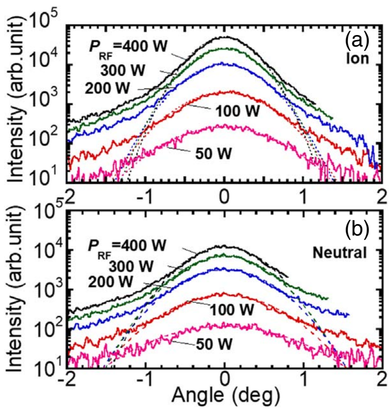

Fig. 3. (Color online) Angular distribution of (a) ion and (b) neutral at p = 4 Pa. RF power is varied from 50 to 400 W.

due to their energy distributions and are difficult to obtain a quantitative value of angular broadening. Hereafter, we focus on the center peak component, i.e., the most intense signal component in the energy distribution, and discuss the distribution width as the quantitative parameter using Gaussian fitting.

If the incident particle has velocity components perpendicular ($v_\perp$) and parallel ($v_\parallel$) to the electrode surface normal, θ_{in} of the particle is

$$\theta_{in} = \tan^{-1}(v_\perp/v_\parallel) \sim v_\perp/v_\parallel \ (\text{rad}). \tag{1}$$

Here, θ_{in} is described in the unit of radian and a small incident angle ($v_\perp/v_\parallel \ll 1$) is supposed. At the sheath edge, ion temperature and ion collision in the pre-sheath determine lateral velocity distribution of ion $f(v_\perp)$. Supposing Gaussian velocity distribution to the lateral direction with *effective* ion temperature (T_i^{eff}) at the sheath edge, the angular distribution of the incident particle is

$$f(\theta_{in}) \propto \exp\left[-\frac{\frac{1}{2}M(\theta_{in}v_\parallel)^2}{kT_i^{eff}}\right] = \exp\left[-\theta_{in}{}^2\frac{E_\parallel}{kT_i^{eff}}\right], \tag{2}$$

where $E_\parallel$ is kinetic energy component to the direction parallel to the surface normal and is

$$E_\parallel = \frac{1}{2}Mv_\parallel{}^2. \tag{3}$$

The above formula shows that angular distribution is again Gaussian and its width is determined by T_i^{eff} at the sheath edge and $E_\parallel$ at the RF electrode. Although, both ions and CX neutrals has energy distribution in $E_\parallel$, it is still worth to adopt Gaussian profile fitting of the angular distribution as an index of angular broadening factor as

$$f(\theta_{in}) \propto \exp\left(-\frac{\theta_{in}{}^2}{\theta_W{}^2}\right). \tag{4}$$

Here, θ_W is index of angular broadening width. Broken curves in Figs. 3(a) and 3(b) show the best-fitted Gaussian profile for each measured angular profile, focusing on the intense center peak. The best-fitted profile well fit to the peak-component irrespective of the RF power.

Figure 4(a) shows a semi-logarithmic plot of ion and neutral peak intensities as a function of the V_{DC}, where the intensities are obtained by integrating the angular distributions supposing a circular beam spot profile. In the figure, both ion and neutral intensities drastically increase by factors of $40 \sim 60$, with increasing the V_{DC} from 0.3 to 0.9 kV. Taking account for the weak dependence of the plasma density on the V_{DC}, the result implies that the MCP sensitivity drastically increases with increasing the incident energy and that the MCP preferentially detects ions and neutrals with their maximum energies. This is consistent with the result of Fig. 2(c), showing the most intense ion signal is at $E_\parallel \sim e(V_P + V_{DC}) \sim eV_{DC}$. Gaussian fittings of the IAD and NAD peaks mean that fitting of the angular profile of higher energy regions. Figure 4(b) shows best-fitted θ_W of ion and neutral profile as a function of the V_{DC}. Both vertical and horizontal axes are indicated in the logarithmic scale. Broadening widths θ_W of ion and neutral are less than 1° and decrease monotonically with increasing the self-bias voltage.

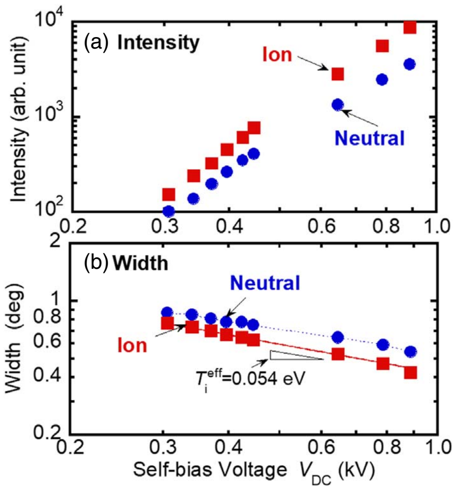

Fig. 4. (Color online) (a) Signal intensities of ion and neutrals as a function of the self-bias voltage. (b) Widths of ion and neutral peaks obtained from best-fitted Gaussian profiles as a function of the self-bias voltage.

Considering that the broadening is determined by the random motion of ions at the sheath edge and incident energies close to their maximum, a decrease in the ion θ_W indicates an increase of the maximum particle energy. From X_S–V_{DEF} relation, the maximum intensity position in Fig. 2(c) corresponds to ion energy close to eV_{DC}. Then, the $\theta_W - V_{DC}$ relation is described as follows,

$$\theta_W = \sqrt{\frac{T_i^{eff}}{V_{DC}}}. \tag{5}$$

The above formula means V_{DC}-θ_W dependence of the ion shows a monotonic decrease with the slope of $-1/2$ in Fig. 4(b). The best-fitted line of the θ_W-V_{DC} relation for the ion is shown by the solid line in Fig. 4(b), and the experimental result well reproduces the relation of Eq. (5). Furthermore, from the fitted line, an effective ion temperature of 0.054 ± 0.005 eV is obtained, taking into account the ambiguity of the maximum ion energy due to "saddle"-structure energy spread.[28,29] So far, ion temperature has been commonly measured by the laser Doppler technique,[30] but this result demonstrates that the IAD measurement is also possible for the ion temperature measurement in the vicinity of the sheath edge. Phelps reviewed detailed cross-section data of Ar^+ collision with Ar and has pointed out that, at high energies above $\sim$1 eV, CX collision is a dominant process than isotropic scattering collisions.[31] At 100 eV, for example, cross-sections of CX and isotropic scattering are $\sim 5 \times 10^{-19}$ m^2 and $\sim 2 \times 10^{-20}$ m^2, respectively. In this study, sheath thickness is comparable to the CX mean free path but is much shorter than the mean free path of isotropic scattering. This means that high-energy neutrals are produced by the CX process, conserving the lateral energy distribution of ions. When CX thermal ions are produced near the sheath edge, they will gain higher energy in the sheath compared with those produced near the electrode. On the other hand, CX-produced neutrals will have higher energy when they are produced near the electrode. Due to the collision process in the sheath, ion flux monotonically decreases with traveling through the sheath, as well as the collision rate of Ar^+ with Ar. This means that the IEDF of CX-produced Ar^+ has a higher intensity in its high energy region, and NEDF of CX neutrals in its low energy region.[14] This is presumably the reason for the wide NADF width compared with that of the IADF.

In conclusion, an experimental apparatus for the angular distribution measurement both for ion and neutral were developed in an RF (powered) electrode of capacitively coupled plasma equipment. Ions and neutrals were extracted into a drift chamber through an orifice on the RF electrode. Electric-field-free space in the drift chamber was confirmed by connecting the drift chamber directly to the RF electrode, and by biasing both components with the RF power at the same time. Neutral and ion beams were separated by an electrostatic ion deflector in the drift chamber. Angular distribution of ions and neutrals were measured by a micro-channel plate so that a two-dimensional beam image can be obtained. Due to the energy dependence of the MCP sensitivity, the high energy component of the energy distribution was preferentially detected by the MCP. Angular distributions of both ion and neutral showed peaked angular profile at low angles below 1° with broader distribution with low intensities. Angular distribution width of the peaked component was evaluated assuming Gaussian distribution. IAD width was proportional to the reciprocal square root of the ion energy, which was in good agreement with an analytic formula supposing a constant effective ion temperature of 0.054 eV. NAD width was always larger than that of ion irrespective of the RF power, suggesting the high energy component of the neutral energy distribution is lower than that of the ion energy distributions.

ORCID iDs Haruka Suzuki https://orcid.org/0000-0002-6877-6417 Hirotaka Toyoda https://orcid.org/0000-0003-2914-4852

1) T. Kinoshita, M. Hane, and J. P. McVittie, J. Vac. Sci. Technol. B **14**, 560 (1996).
2) G. S. Hwang and K. P. Giapis, J. Vac. Sci. Technol. B **15**, 70 (1997).
3) M. Boufnichel, S. Aachboun, F. Grangeon, P. Lefaucheux, and P. Ranson, J. Vac. Sci. Technol. B **20**, 1508 (2002).
4) M. Boufnichel, S. Aachboun, P. Lefaucheux, and P. Ranson, J. Vac. Sci. Technol. B **21**, 267 (2003).
5) J. K. Lee, I. Y. Jang, S. H. Lee, C. K. Kim, and S. H. Moon, J. Electrochem. Soc. **157**, D142 (2010).
6) A. P. Mahorowala, H. H. Sawin, R. Jones, and A. H. Labun, J. Vac. Sci. Technol. B **20**, 1055 (2002).
7) J. Saussac, J. Margot, and M. Chaker, J. Vac. Sci. Technol. A **27**, 130 (2009).
8) K. H. A. Bogart, F. P. Klemens, M. V. Malyshev, J. I. Colonell, V. M. Donnelly, J. T. C. Lee, and J. M. Lane, J. Vac. Sci. Technol. A **18**, 197 (2000).
9) R. J. Hoekstra, M. J. Kushner, V. Sukharev, and P. Schoenborn, J. Vac. Sci. Technol. B **16**, 2102 (1998).
10) M. A. Vyvoda, M. Li, D. B. Graves, H. Lee, M. V. Malyshev, F. P. Klemens, J. T. C. Lee, and V. M. Donnelly, J. Vac. Sci. Technol. B **18**, 820 (2000).
11) M. Moriyama, N. Nakahara, A. Mitsuya, H. Suzuki, K. Kurihara, D. Iino, H. Fukumizu, and H. Toyoda, Jpn. J. Appl. Phys. **59**, SJJB03 (2020).
12) M. Moriyama, N. Nakahara, K. Kurihara, D. Iino, H. Fukumizu, H. Suzuki, and H. Toyoda, Jpn. J. Appl. Phys. **60**, 016001 (2021).
13) B. E. Thompson, H. H. Sawin, and D. A. Fisher, J. Appl. Phys. **63**, 2241 (1988).
14) N. Mizutani and T. Hayashi, Jpn. J. Appl. Phys. **38**, 4206 (1999).
15) Z. Saiqian, D. Zhongling, and W. Younian, Plasma Sci. Technol. **14**, 958 (2012).
16) R. A. Gottscho, J. Vac. Sci. Technol. B **11**, 1884 (1993).
17) L. L. Raja and M. Linne, J. Appl. Phys. **92**, 7032 (2002).
18) S. Wang, X. Xu, and Y. N. Wang, Phys. Plasmas **14**, 113501 (2007).

19) Z. L. Dai, X. Xu, and Y. N. Wang, Phys. Plasmas **14**, 013507 (2007).
20) D. Kim and D. J. Economou, IEEE Trans. Plasma Sci. **30**, 2048 (2002).
21) Y. Takao, K. Matsuoka, K. Eriguchi, and K. Ono, Jpn. J. Appl. Phys. **50**, 08JC02 (2011).
22) M. Shihab and T. Mussenbrock, Phys. Plasmas **24**, 113510 (2017).
23) J. Liu, G. L. Huppert, and H. H. Sawin, J. Appl. Phys. **68**, 3916 (1990).
24) J. R. Woodworth, M. E. Riley, D. C. Meister, B. P. Aragon, M. S. Le, and H. H. Sawin, J. Appl. Phys. **80**, 1304 (1996).
25) N. Mizutani and T. Hayashi, J. Vac. Sci. Technol. A **19**, 1298 (2001).
26) S. Sharma, D. Gahan, P. Scullin, S. Daniels, and M. B. Hopkins, Rev. Sci. Instrum. **86**, 113501 (2015).
27) E. Aydil, B. O. M. Quiniou, J. T. C. Lee, J. A. Gregus, and R. A. Gottscho, Mat. Sci. Semicon. Process. **1**, 75 (1998).
28) P. Benoit-Cattin and L. A. Bernard, J. Appl. Phys. **39**, 5723 (1968).
29) E. Kawamura, V. Vahedi, M. A. Lieberman, and C. K. Birdsall, Plasma Sources Sci. Technol. **8**, R45 (1999).
30) G. A. Hebner, J. Appl. Phys. **80**, 2624 (1996).
31) A. V. Phelps, J. Appl. Phys. **76**, 747 (1994).